What can we learn from over 100,000 *Escherichia coli* genomes?

Kaleb Abram[1]*, Zulema Udaondo[1]*, Carissa Bleker[2,3], Visanu Wanchai[1], Trudy M. Wassenaar[4], Michael S. Robeson II[1], Dave W. Ussery[1#]

[1]Department of Biomedical Informatics, University of Arkansas for Medical Sciences, Little Rock, Arkansas, USA

[2]The Bredesen Center for Interdisciplinary Research and Graduate Education, University of Tennessee, Knoxville, TN, USA

[3]Department of Electrical Engineering and Computer Science, University of Tennessee, Knoxville, TN, USA

[4]Molecular Microbiology and Genomics Consultants, Zotzenheim, Germany

#Corresponding author: DWUssery@uams.edu

*These authors contributed equally

Running title: Insights from over 100,000 *E. coli* genomes

Keywords: *Escherichia coli*, phylogroup, pangenome, core genes, comparative genomics, population structure, taxonomy, Mash, phylotype, *Shigella*, phylogeny, phylotype

ABSTRACT

The explosion of microbial genome sequences in public databases allows for large-scale population genomic studies of bacterial species, such as *Escherichia coli*. In this study, we examine and classify more than one hundred thousand *E. coli* and *Shigella* genomes. After removing outliers, a semi-automated Mash-based analysis of 10,667 assembled genomes reveals 14 distinct phylogroups. A representative genome or medoid identified for each phylogroup serves as a proxy to classify more than 95,000 unassembled genomes. This analysis shows that most sequenced *E. coli* genomes belong to 4 phylogroups (A, C, B1 and E2(O157)). Authenticity of the 14 phylogroups described is supported by pangenomic and phylogenetic analyses, which show differences in gene preservation between phylogroups. A phylogenetic tree constructed with 2,613 single copy core genes along with a matrix of phylogenetic profiles is used to confirm that the 14 phylogroups change at different rates of gene gain/loss/duplication. The methodology used in this work is able to identify previously uncharacterized phylogroups in *E. coli* species. Some of these new phylogroups harbor clonal strains that have undergone a process of genomic adaptation to the acquisition of new genomic elements related to virulence or antibiotic resistance. This is, to our knowledge, the largest *E. coli* genome dataset analyzed to date and provides valuable insights into the population structure of the species.

E. coli is a common inhabitant of the gastrointestinal tract of warm-blooded organisms, and can also be found in soil and freshwater environments[1]. The species is comprised of both commensal and pathogenic strains which can cause disease in a wide variety of hosts. In humans, pathogenic *E. coli* strains are a leading cause of diarrhea-associated hospitalizations[2]. Some of the reasons why *E. coli* is intensely studied are: rapid growth rate in the presence of oxygen, easy adaptation to environmental changes, and the relative ease with which it can be genetically manipulated[3]. Genomic diversity of the species, to which the genus *Shigella* has been proposed to be included[4,5], is reflected by the existence of several phylogenetic groups (phylogroups) that have been identified using a variety of different methods[6–8].

Historically, four phylogroups have been recognized as detected by triplex PCR: A, B1, B2, and D[6,8] and three more were added later[9]: phylogroups C (closest relative to B1), F (as a

49 sister group of phylogroup B2), and E to which many D members were reassigned. Some studies
50 have further subdivided these phylogroups with subdivisions of F and D, and separate
51 phylogroups for *Shigella* species[10]. Recently, Clermont *et al.*[11] characterized phylotype G using
52 multiplex PCR as an intermediate phylogroup between B2 and F. These phylogroups are thought
53 to be monophyletic[8,10] and partially coincide with different ecological niches and lifestyles.
54 Moreover, phylogroups differ in metabolic characteristics, the presence of virulence genes, and
55 also in antibiotic resistance profiles[8,12–14].

56 Here we describe a comprehensive analysis of over 100,000 publicly available genome
57 sequences, consisting of 12,602 assembled genomic sequences from GenBank and over 125,000
58 unassembled genome sequences from the Sequence Read Archive (SRA). This study combines
59 whole genome sequences (WGS) and SRA unassembled genomes using high-performance
60 computing resources to conduct, to our knowledge, the largest analysis to date of the population
61 structure of *E. coli*. We have assessed the genomic similarities and differences between
62 phylogroups to characterize the genetic heterogeneity of these different phylogenetic lineages.
63 We have also identified 14 'medoid'[15] genomes that can be considered as the genetic 'center' of
64 each of the phylogroups in our dataset and can be used as a representative sequence for the
65 associated phylogroup. Furthermore, this study has application to the fields of public health and
66 medical science as it provides detailed information of the existing diversity of the *E. coli* species
67 enabling public health researchers to identify pathogenic strains that belong to the same genetic
68 lineage appearing in outbreaks at different temporal and geographical locations.

69

70 **RESULTS**

71 ***Mash analysis of E. coli genomic sequences reveals 14 phylogroups.*** As illustrated by Fig. 1,
72 Mash-based clustering methodology differentiated 14 different phylogroups consisting of *E. coli*:
73 G, B2-1, B2-2, F, D1, D2, D3, E2(O157), E1, A, C, B1, and *Shigella*: Shig1 and Shig2 (ordered
74 as in Fig. 1) by using a cutoff in which the last literature accepted phylogroup became visible.
75 The phylogroups Shig1 and Shig2 exclusively contained *Shigella* species, but *Shigella* sp.
76 genomes were also found in phylogroups A, B1, B2-2, D2, D3, E1, and F (Supplementary Figure
77 1). Genomes within each of these phylogroups share a lower intragroup distance (meaning higher

genetic similarity) than they do to any other genome within the rest of the species. In addition, the genetic relatedness between any phylogroup and the rest of the species is graphically shown. For example, phylogroups A, B1, and C are more closely related to each other than any one of these phylogroups are to B2-1 or B2-2, as illustrated by lower Mash distances between phylogroups A, B1, and C compared to B2-1 or B2-2. Fig. 1 also illustrates the phylogroup substructure or intragroup genetic relatedness. E2(O157), Shig1, and Shig2 harbor the most homogeneous genomes, which can be seen in the limited range of Mash distances within these phylogroups. On the other hand, B1 and B2-2 are more heterogenous as shown by numerous smaller dark teal squares that correspond to clusters of genomes that have a lower Mash distance between them compared to the rest of the genomes in that phylogroup. The relative abundance of phylogroup sequences with respect to each other can also be observed in Fig. 1. G has the smallest number of genomes sequenced and B1 has the largest number of sequenced genomes in the assembled dataset.

Microreact[16] was utilized to further explore the results of the Mash-based analysis, as this provides an easy medium for researchers to determine the closest genetic neighbors to any genome in this dataset. Additionally, due to the inclusion of some clinically relevant outbreak strains, such as O157:H7, O104:H4, and O104:H21, basic retroactive genomic surveillance is possible by identifying strains of known outbreaks and noting their nearest neighbors. This data is available on Microreact at: https://microreact.org/project/10667ecoli/4098eb8c.

Currently sequenced E. coli and Shigella species can be represented by 14 medoid genomes. We were able to determine that 14 representative genomes can serve as the medoid or the "genomic center" of each phylogroup based on the 10,667 analyzed genomes. Our results show high correspondence with the recently proposed evolutionary scenario for the *E. coli* species[17] (Fig. 2). The Cytoscape analysis showed that the two B2 phylogroups are the most genetically distinct from the remainder of the species as they separate earliest from the other phylogroups. At the final Mash value cutoff of 0.0095, the C and B1 phylogroups become the last two groups to separate. This last split is indicative of the relatively large shared genomic content between these two phylogroups. The resultant Cytoscape graphs were collected into a video available as Supplementary Video 1, and a collection of stills is available on the service figshare via

108 http://dx.doi.org/10.6084/m9.figshare.11473308. Between the initial Cytoscape frame and the
109 final frame, the number of genomes represented decreased by 43% while the edges (connections
110 between genomes and medoids) decreased by 96%. As the cutoff decreases, some genomes are
111 no longer represented in the Cytoscape analysis due to having no Mash distance equal to or less
112 than the applied cutoff. As expected, the overall interconnectivity between the different
113 phylogroups drops significantly with the cutoff, but intraconnectivity within the phylogroups
114 does not. Upon visualization and inspection of the data via Cytoscape, we could verify that each
115 medoid is representative of its entire phylogroup and therefore the 14 medoids are suitable to be
116 used for decreasing visual complexity without sacrificing accuracy. Information about the 14
117 found medoids is available in Supplementary Table 2.

118 ***Most sequenced E. coli genomes belong to 4 phylogroups.*** The use of medoid genomes as a
119 proxy to classify more than 100,000 genomes revealed that most of the currently sequenced *E.*
120 *coli* strains belong to 4 phylogroups. Around two-thirds (67%) of the analyzed SRA reads were
121 predicted to belong to four phylogroups: A (23%), C (15%), B1 (15%), and E2(O157) (14%).
122 This large disparity in phylogroup diversity in the SRA dataset most likely reflects the research
123 interests of the scientific and medical communities. Strains belonging to phylogroups B1, C, and
124 E2(O157) are often pathogenic and of interest to medical research, while phylogroup A includes
125 strains frequently used in the laboratory (*e.g.*, strain K-12) or genetically modified strains (such
126 as strains BL21 and REL606). Similarly, a little over two-thirds (70%) of the 10,667 assembled
127 genomes also belong to four phylogroups: B1 (28%), A (21%), B2-2 (13%) and Shig2 (8%).
128 However, in the assembled genomes dataset, phylogroup C is only about 5% and E2(O157) is
129 about 7%. It is somewhat unexpected that the assembled genomes have a different distribution of
130 genomes than the unassembled dataset; however, this could be due to how fast and inexpensive
131 unassembled genomes are to produce and their utility in genomic surveillance of outbreaks. A
132 breakdown of the results for the SRA analysis including the number of medoid hits below the
133 cutoff is summarized in Supplementary Table 3. Additionally, a collection of heatmaps with
134 different membership cut-offs, ranging from one to 14 phylogroups can be found in
135 Supplementary Figure 2.
136

137 ***Members of Mash phylogroups possess different genomic features.*** Since Mash values provide
138 a measure of similarity via distance between pairs of genomes, the phylogroups of Fig. 1 are the
139 consequence of differences/similarities in the genetic content of each genome with respect to the
140 rest of the genomes included in the analysis. Differences in genome size and percentage of GC
141 content between phylogenetic groups were observed (Supplementary Figure 3) and statistical
142 tests were performed by ANOVA and Tukey's multiple comparison test (see Methods and
143 Supplementary Table 4). According to these analyses, genomes from phylogroups Shig1, Shig2,
144 A, B1 and B2-1 are significantly smaller in size than phylogroups E2(O157) and C ($P<0.01$).
145 The smaller genome size of the strains from both *Shigella* phylogroups is indicative of a
146 reductive evolution of the genomes of these strains as previously described[18] by Weinert and
147 Welch which is mainly driven by their role as intracellular pathogens. Other enteroinvasive *E.*
148 *coli* strains such as serotypes O124, O152, O135 and O112ac were classified inside phylogroups
149 A (typically engineered, lab, and commensal strains) and B1 (often environmental strains) which
150 are the most heterogeneous phylogroups due to the diverse nature of their strains in terms of their
151 environmental niche. This heterogeneity is also reflected in the large ranges of genome size and
152 GC content of these two phylogroups. However, reduced genome size is not associated with
153 pathogenicity *per se*, as the large genomes of E2(O157) and C phylogroups illustrate. Larger
154 genome sizes associated with virulence may result from the accumulation of virulence genes in
155 prophages, pathogenicity islands, and plasmids[19]. Significant genomic differences in GC content,
156 with respect to other phylogroups were only found for the two *Shigella* phylogroups ($P<0.01$),
157 which also agrees with an ongoing purifying or negative selection occurring in these genomes[18].
158 These characteristics might reflect the different evolutionary strategies and opposite selection
159 pressures as a consequence of adaptation to diverse niches in which the different phylogroups
160 have evolved[20].

161 ***Level of preservation of homologous genes varies between phylogroups.*** To evaluate the
162 existence of functional traits associated with each of the phylogroups, we conducted pangenome-
163 approach based analyses using the proteomes of the 10,667 assembled genomes. In addition,
164 separate pan and core genomes were calculated for the 14 individual phylogroups. This approach
165 allows us to highlight the unique proteomic cores of each phylogroup, which in turns helps to

166 define their distinct biology. The total set of genes of the species (pangenome) is comprised of
167 135,983 clusters of homologous proteins (Table 1). By testing the cutoffs for core genome
168 conservation from 90% to 99% of the genomes (Supplementary Fig. 4) we concluded that, while
169 the traditional cutoff for core genome calculation of 95% of genomes would suffice, a cutoff of
170 97% can minimize erroneous false positive core genes thus providing a more stringent result.
171 Therefore, we defined the core genome as homologous genes shared by at least 97% of the
172 genomes ($^{TOT}core_{97}$), which produced a core genome of 2,663 clusters (1.96% of the total
173 pangenome clusters). The $^{TOT}core_{97,}$ colored green in Fig. 3a, contains the well-preserved genes
174 that define the species, and for the shortest sequenced genomes (e.g. *Escherichia coli* str. K-12
175 substr. MDS42, phylogroup A), these constitute approximately 74% of their gene content; in
176 contrast, for the largest genomes (e.g. *E. coli* Ec138B_L1, phylogroup A) this fraction is only
177 about 32%.

178 By defining phylogroup-specific core genomes ($^{PHY}core_{97}$) it becomes apparent that large
179 differences exist between the levels of gene preservation for each of the phylogroups (Fig. 3a).
180 Predictably, the phylogroup with the largest number of $^{PHY}core_{97}$ gene clusters is E2(O157). Not
181 only do its members have large genomes, but this phylogroup is also very homogeneous as it
182 mostly contains *E. coli* O157:H7 strains that have a clonal origin[21]. Relatively large $^{PHY}core_{97}$ are
183 also observed for phylogroups C, harboring strains of clinically relevant non-O157
184 enterohemorrhagic (EHEC) serotypes such as O111 and O26, and for phylogroup Shig2, whose
185 members have relatively short genomes as it is mainly composed of *S. sonnei* strains, suggesting
186 that these phylogroups are relatively homogeneous which increases the size of the core genome
187 in turn decreasing the fraction of accessory genes. At the other end of the spectrum, the
188 phylogroup with the smallest core genome is Shig1 followed by phylogroups B1, E1, and A
189 (Table 1). The small core genome of Shig1 is related to its small genome size, while more
190 numerous phylogroups A, E1, and B1 contain more diverse members, resulting in a larger
191 fraction of accessory genes and a smaller phylogroup-specific core. This observation concurs
192 with the tendency of other environmental strains that usually present open pangenomes with
193 higher ratios of accessory and unique genes[22,23]. Nevertheless, although Shig1 phylogroup has
194 the smallest number of core genes, this number represents almost 29% of the total clusters found

195 in this phylogroup (Table 1), which is the highest ratio of core gene clusters per phylogroup-
196 specific pangenome of the analysis. Phylogroups with fewer members can also produce larger
197 core genome fractions with respect to their pangenome due to sampling biases. Phylogroup G
198 was recently described by Clermont *et al.*[11] as a multidrug resistant extra-intestinal pathogenic
199 phylogroup (ExPEC). G strains are closely related to strains from the B2 complex, and are
200 commonly isolated from poultry and poultry meat products, which coincides with our analyses
201 and available metadata. Although phylogroup G has the fewest number of strains in our dataset,
202 we believe that the high core/pan ratio of this phylogroup is due to the overabundance of the
203 sequence type ST117 (79% of the strains) which makes this phylogroup quite homogeneous.
204 Based on these observations we conclude that the relative ratio of $^{PHY}core_{97}$ to the total
205 phylogroup pangenome clusters is a measure of the intragroup diversity.

206 To analyze the distribution of the 14 phylogroups in terms of their shared genetic content,
207 a two-dimensional projection of the presence or absence of all protein families (complete
208 pangenome) for the 10,667 assembled genomes was represented by a Principal Coordinate
209 Analysis (PCoA) as shown in Fig. 3b. An initial observation of the PCoA plot is that
210 phylogroups segregated on the left side of the Y axis (B2-1, B2-2, G, F, D1, D2, D3) comprise
211 phylogroups that contain large numbers of strains labeled as extra-intestinal *E. coli* strains
212 (ExPEC)[11,13,24]. The observed overlap of B2-1 with the B2-2 phylogroup in Fig. 3b could be due
213 to their shared evolutionary history. For example, *in silico* MLST analyses shows that at least
214 80% of B2-1 strains belong to the sequence type ST131, a multidrug resistant clonal group of
215 ExPEC that recently emerged from the B2-2 phylogroup[25]. This explains the high degree of
216 homogeneity of B2-1 phylogroup. Moreover, strains characterized as ST131 were not found in
217 other phylogroups in our dataset. It appears that the rapid and differential acquisition of unique
218 virulence and mobile genetic elements by ST131 strains[26] make it possible to discriminate
219 between B2-1 (mainly ST131 strains) and B2-2 phylogroups using WGS approaches such as the
220 one used in this work.

221 While most of the phylogroups seem to have a relatively horizontal distribution within
222 the PCoA plot, phylogroups E2(O157) and Shig2 show the most striking differences in regards
223 to their vertical distribution with respect to the rest of phylogroups. As commented before, Shig2

224 and E2(O157) are very homogeneous phylogroups, with large $^{PHY}core_{97}$ that contain over 1,000
225 more protein families than the $^{TOT}core_{97}$ of the species. These phylogroup-specific core genes
226 could contain genetic signatures that are not present in the core genome of other phylogroups,
227 and therefore would confer to all phylogroup members with intrinsic and distinguishable traits
228 making them "traceable" in terms of genetic content from the rest of phylogroups.

229 To represent the existence of unique phylogroup-specific core genes we made a
230 comparison only considering the 14 $^{PHY}core_{97}$ and re-clustered them using the same parameters
231 as in the previous pangenome analyses. Fig. 3c is a representation of the sorted resultant clusters,
232 placing clusters from the $^{TOT}core_{97}$ first, followed by the $^{PHY}core_{97}$ clusters from the rest of
233 phylogroups. Sorting the clusters in this way, highlights clusters of core genes that are exclusive
234 to the $^{PHY}core_{97}$ of a given phylotype. As can be observed, phylogroups E2(O157) and Shig2
235 possess the highest proportion of unique core genes (protein family clusters (columns) colored in
236 purple that are not present in the other phylogroups), followed by C, B2-1, and Shig1
237 phylogroups. Well-defined phylogroup unique core genes were also found for phylogroups D3
238 (uropathogenic multidrug resistant strains, mainly ST405 and ST38) and D1 (uropathogenic
239 multidrug resistant strains, predominantly ST69). A list of the phylogroup unique core genes
240 found and represented in Fig. 3c along with their associated functional features can be found in
241 Supplementary Table 5. Some of these clusters of genes comprise interesting characteristics such
242 as: a unique set of genes for synthesis of flagella only present in all strains belonging to the C
243 phylogroup, a complete set of genes for the transport of iron and ribose present in all members of
244 phylogroup E2(O157), and a set of genes for the synthesis of siderophores in B2-1 phylogroup
245 (Supplementary Table 5). The presence of unique-core gene clusters belonging to the $^{PHY}core_{97}$
246 of most phylogroups supports the existence of 14 distinguishable phylogroups within the species.
247 These genetic signatures might also have applications in public health as they could be utilized
248 for typing purposes.

249 However, not all phylogroups harbor phylogroups-specific genes. Phylogroups A and B1
250 have the weakest unique core signatures observed (along with D2 and E1 phylogroups), which
251 could be explained by the heterogeneous nature of both phylogroups. Although B1 is comprised
252 of strains isolated from environmental sources, it also contains enteropathogenic strains (EPEC),
253 EIEC strains and most of the *Shigella* strains, such as *S. boydii* and *S. dysenteriae,* that were not

classified by Mash analysis in Shig1 or Shig2 phylogroups (Supplementary Fig. 1 and Microreact data). These *Shigella* strains can be observed in the PCoA plot as the B1 small cluster just on top of the Shig1 cluster. It is interesting to note that, although phylogroups A and B1 are well-defined and described phylogroups, they are also considered as sister phylogroups with a shared evolutionary history[7,13,27] which is represented by their partial overlap observed in Fig. 3b and their late segregation observed in the Supplementary Video 1 and Fig. 2b at a Mash distance of 0.0115.

Phylogroups evolve with different gain/loss rates of protein families. Since the medoids were shown to be suitable representative entities of the 14 phylogroups and the $^{TOT}core_{97}$ genome was established, a robust phylogeny analysis could now be performed based on the concatenated independent alignment of 2,613 $^{TOT}core_{97}$ gene clusters without paralogs and a maximum likelihood approach (Fig. 4a). The obtained phylogenetic tree, along with a matrix containing the number of homolog genes per protein family for each representative genome, were used to measure family sizes and lineage specific events applying an optimized gain-loss-duplicated model. Differences in gene content between the medoids lead to the observation that the different phylogroups have evolved with different gain/loss/duplication rates of protein families (Fig. 4b). Relatively high ratios of gene expansion were observed for phylogroups Shig1, Shig2, C, and B2-1. As expected due to their smaller genomes, Shig1 and Shig2 possess the highest ratios of gene loss, while Shig1, C, and Shig2 have the highest rates of gene duplication. On the other hand, phylogroups A, B1, D3, and F have the lowest rates of gene gain, indicating these phylogroups have undergone limited gene expansion. It is also interesting to note is that phylogroups D2, B1, and G have much lower rates of gene duplication compared to the other phylogroups. In short, all phylogroups showed differential gain/loss duplication ratios of gene families, even those that share a presumed ancestral history, such as the D phylogroups. As stated before, D1 and D3 phylogroups comprise mainly UPEC strains and they are mainly represented by one or two predominant sequence types. Conversely, D2 strains are typically isolated from non-human sources with a large variation of sequence types.

Discussion

Mash-based analysis provides a fast and highly scalable K-mer based approach that can be used on extremely large sets of genomes. Based on more than one hundred thousand genomes, the population structure of *E. coli* species appears to be more diverse than currently thought. The methodology applied here detected 14 phylogroups with a remarkably unequal distribution of membership in regards to the number of genomes per phylogroup. The current bias in sequencing data decreases the probability of finding the genetic signatures that captures the relative homogeneity of all members of the phylogroups. As a consequence, less numerously represented phylogroups may actually contain additional, as yet unidentified phylogroups or sub-structures within them and currently conclusions about their open or closed nature cannot be accurately drawn.

The presence of multiple phylogroups that share pathogenic characteristics and even share equivalent environmental niches, such as the D and B2 phylogroups, is indicative of faster evolutionary forces related to the pathogenic lifestyle of these strains that could be driven by the acquisition of virulence factors, recombinations, and interactions with the local flora of the host. While the analysis of gain/loss/duplication rates of the phylogroups does not assess the rate of mutation, the k-mer based Mash analysis can capture subtle differences in sequence similarity making these forces traceable. According to our analysis, the emergence of new phylogroups of *E. coli* is due to the pathogenic specialization of previously established phylogroups, such as phylogroups B2-1, D1, D2, and D3. These phylogroups could have acquired new genetic material causing the rest of the genome to adapt thus producing changes that are detected by WGS techniques such as Mash but are not detected by more target-restricted methods such as PCR. We therefore conclude that the use of WGS data with Mash to assess a bacterial species' genetic sub-structure is essential to increasing our understanding of bacterial diversity.

312 **METHODS**

313 ***Data Acquisition and Cleaning***. To conduct the analysis, 12,602 genome sequences labeled
314 either *Escherichia* or *Shigella* were downloaded from GenBank on 26 June, 2018 using batch
315 Entrez and the list of GCAs accession numbers from NCBI Genome database (including plasmid
316 sequences when applicable). This dataset (Supplementary Table 1) was cleaned to obtain an
317 informative and diverse set of 10,667 *E. coli* and *Shigella* genomes that captures the diversity of
318 the species as sequenced to date. In addition to the GenBank genomes, a total of 125,771 read
319 sets labeled as either *E. coli* or *Shigella* were downloaded from the SRA database. After cleaning
320 the dataset, we utilized Mash[28], a program that approximates similarity between two genomes in
321 nucleotide content, and an in-house Python script to create a matrix of distances for all 10,667
322 genomes. This matrix was then clustered using hierarchical clustering after converting the Mash
323 distance to a Pearson's Correlation Coefficient distance to ensure that clustering results were
324 based on a genome's overall similarity to the whole species.

325 To evaluate the quality of the data set, various sequence quality scores were calculated as
326 described[29] by Land *et al*.. Following the recommended quality score cutoff value of 0.8, the
327 dataset was filtered to include only genomes with a total quality score of 0.8 or higher. Applying
328 the same cutoff value to the sequence quality score alone resulted in an extremely restricted
329 dataset that no longer addressed the goals of this study. Genome size was restricted to greater
330 than 3 Mb and less than 6.77 Mb to remove questionably sized genomes, which could be due to
331 contamination or modified genomes that are not representative of the natural *E. coli* species.
332 After applying these two steps, 10,855 genomes remained in the assembled genome dataset for
333 analysis.

334 To further clean the dataset, we filtered genomes that were outside the statistical distribution of
335 Mash distances within the dataset. Assuming that *Shigella* species are all members of *E. coli*, we
336 decided to use type strains for the *Escherichia* and *Shigella* genera (accession numbers
337 GCA_000613265.1 and GCA_002949675.1, respectively) to quickly filter the set of 10,855
338 genomes for erroneous or low-quality genomes that may have slipped through the previous
339 cleaning steps. The Mash values of the 10,855 genomes compared to each type strain were

340 broken into percentiles ranging from 10% to 99.995%. A cutoff percentile of 98.5% was
341 determined to provide sufficient cleaning without risking a large loss of data (data not shown)
342 and was applied to each type strain Mash value set. Genomes that were found in both sets after
343 filtering were retained to produce the final dataset of 10,667 genomes.

344 ***Microreact***. Microreact[16], was utilized to visualize the resultant clustering of the Mash data as
345 this provides an easy and fast medium to further explore the results of the analysis. To leverage
346 the search capabilities of Microreact, we mapped metadata found for our dataset from the
347 database PATRIC[30] (downloaded on 2019/6/20). This allows the exploration of our results using
348 a number of shared characteristics and queries such as "geographic location" or "serovar" that
349 although outside the scope of the current study, could be used as a topic for future analyses to
350 increase our understanding of *E. coli* species.

351 ***Mash and Clustering Analysis.*** Genetic distances between all 10,667 genomes were calculated
352 using 'mash dist' with a k-mer size of 21 and a sampling size of 10,000. The resulting output was
353 converted into a distance matrix with assembly accession numbers as columns and rows. To
354 improve the clustering results and to provide a standard metric that allows comparison of
355 different analytical methods, we converted the Mash distance value into a similarity measure via
356 the Pearson correlation coefficient[31]. This returns values ranging from -1 (total negative linear
357 correlation) to 1 (total positive linear correlation), where 0 is no linear correlation. Since
358 clustering-based methods require a distance measure, the values were subtracted from 1 to
359 convert them into a distance measure. These distance measures were then clustered in R using
360 'hclust' and the 'ward.D2' method. A clustered heatmap was generated using the hclust
361 dendrogram to reorder the rows and columns of the distance matrix within the heatmap, while
362 values from the raw distance matrix of Mash distances were mapped to color. To determine the
363 height to cut the hclust dendrogram and to accurately predict phylogroups that optimally
364 overlapped with existing phylogroups, we compared multiple different cutoff values and
365 methods to obtain cutoff values. Taking the maximum height present in the hclust dendrogram
366 and multiplying it by 1.25×10^{-2} was found to provide both accurate predictions and a standard
367 method that scales with the data supplied. Sufficient accuracy was defined by the cutoff at which

368 the last literature accepted phylogroup was visible, in this case representing the C phylogroup
369 splitting off from B1. Some detailed results of both the cutoff percentile and hclust height testing
370 are included for 10,667 genomes in Supplementary Table 5.

371 ***Medoid selection for species representation***. Using the Mash values for the entire species, a
372 medoid was defined for each phylogroup. The medoid is the "real" center of the phylogroup, as it
373 has to exist within the dataset, and was chosen as the genome that has the lowest average
374 distance to all other genomes in its phylogroup. We subsequently tested if one genome from each
375 of the phylogroups would be enough to accurately classify any given genome sequence claimed
376 to be *E. coli* or *Shigella*. The 'aggregate' function of R was used to find the mean across each
377 phylogroup. Isolating each phylogroup, reclustering, and calculating the medoid did not yield as
378 accurate results as calculating the medoid per phylogroup with respect to the entire 10,667
379 genome dataset.

380 ***Addition of SRA reads.*** The keywords "*Escherichia coli*" and "*Shigella*" filtered with "DNA"
381 for biomolecule and "genome" for type was used to retrieve SRA IDs from the NCBI SRA
382 database on March 22, 2019. For large scale data transfer, these SRA genomes were downloaded
383 using the high throughput file transfer application Aspera (http://asperasoft.com). To ease
384 computational and organizational load, the 125,771 read sets obtained from the SRA were
385 divided into five subsets of different sequencing technologies: 3 Illumina paired read sets, 1
386 mixed technology with paired reads, and 1 mixed technology with single reads. The 5 sets of
387 reads were then converted from fastq to fasta format to be processed by Mash using a python
388 script which removed all non-sequence data from the fastq file.

389 The SRA sequence reads were sketched using Mash (v2.1) and the same k-mer and sketch
390 sample size as the 10,667 dataset. This version change was due to the addition of read pooling in
391 the read mode which automatically joins paired reads, eliminating the need to concatenate or
392 otherwise process paired read sets. All read sets were sketched individually so that read sets that
393 caused an error when sketching were dropped from the analysis before sketching. A total of
394 23,680 raw reads could not be sketched. The -m setting was set to 2 to decrease noise in the
395 sketches of the reads. After sketching the reads within the subsets, all sketches were

concatenated into a sketch for that subset using the paste command of Mash. The concatenated sketch of each subset was then compared to the 14 medoids using Mash dist. As all five subsets had the same reference, the distance output from each subset was concatenated to one file. This single SRA distance output file was then analyzed to evaluate the quality of the SRA dataset. Due to how distances are calculated, Mash can consistently flag genomes of very low quality since the major basis of a Mash value is how many hits are present out of sketches sampled. The top 5 most numerous distances of the SRA read sets corresponded to 0 to 4 hits of the possible 10,000 sketches per genome. This indicates the presence of extremely low-quality samples within the SRA dataset. A histogram of the SRA Mash distance results was created to analyze the distribution of Mash distances of the entire 102,091 SRA dataset (results not shown). A final Mash distance cutoff of 0.04 was chosen based on the maximum Mash value in the 10,667 whole set that was 0.0393524. Although this low cutoff might potentially eliminate useful information, it insured quality of the SRA dataset. This retained 95,525 reads that had at least one Mash distance to a phylogroup medoid within the chosen cutoff.

The distance output was transferred into a matrix with reads as columns and rows containing a phylogroup medoid. For each read the smallest Mash distance to a medoid was identified, and the corresponding medoid noted (Supplementary Table 3). We then created a distance matrix from the Mash distance output of the 95,525 reads that met the above cutoff with reads as rows and medoids as columns. Due to computational load this distance matrix was loaded into Python 3 instead of R. A clustered heatmap was made using Seaborn, Matplotlib, and Scipy with the 'clustermap' function. Instead of clustering both rows and columns, columns (phylogroups) were ordered the same as Fig. 1 and rows were sorted as follows: number of hits to phylogroups (ascending = True) and Mash distance (ascending = False). This provided a quick visualization method for the SRA dataset with a consistent sorting criterion to make comparison between Fig. 2c and the Supplemental heatmaps much easier.

Cytoscape visualization. The Mash distance matrix of the 10,667 genomes was filtered to include only the 14 medoids along the columns. This filtered matrix was transformed into a new 3 column matrix where the first column contains the identifier for a genome to be compared to

424 the medoid present in the second column. The third column contains the Mash value for that
425 pairwise comparison. A sliding cutoff ranging from 0.04 to 0.0095 with increments of 0.005 was
426 applied to the Mash value column and rows with values above the sliding cutoff for an iteration
427 were removed. These data tables were imported into Cytoscape (version 3.7.1) with the first
428 column as the source node and the medoid column as the target node. The Prefuse Force
429 Directed Weighted layout was then applied to the network with the Mash distance serving as the
430 weight. Phylogroup membership was mapped with a metadata table and colors were assigned
431 based on the colors used in Fig. 1. For each cutoff the resultant graph was output as an SVG. All
432 SVGs were then compiled into a video to ease visualization of the Cytoscape graphs.

433 ***Statistical analysis of genome sizes and percent GC content.*** Genome sizes and percent of GC
434 content was calculated using the 'infoseq' package from EMBOSS suite v6.6.0.0. A dataframe
435 with sequence ID, percentage of GC content, genome size, and phylogroup ID was made.
436 Library 'ggplot2' from R was used to plot genome sizes and GC content. Library 'dplyr' from R
437 was used to perform analysis of Variance ANOVA test and Tukey HSD tests. The homogeneity
438 of variances was tested using Levene's test and the normality assumption of the data was
439 checked using Shapiro-Wilk test. As some of the groups didn't meet the criteria of the
440 assumption of normality, Kruskal-Wallis test was performed as well as non-parametric
441 alternative to one-way ANOVA. Kruskal-Wallis test rejected both null hypothesis (means of
442 genome size or percent of GC content are similar between the different phylogroups), with p-
443 value $< 2.2e^{-16}$ in both cases. Raw results from these tests are available in Supplementary Table
444 5.

445 ***Pangenome analyses and clustering.*** All 10,667 genomes were reannotated using Prokka[32]
446 v1.13, with parameters: --rnammer --kingdom Bacteria --genus *Escherichia* –species *coli* --gcode
447 11. All protein-coding sequences (n=51,400,905) were clustered using UCLUST from
448 USEARCH[33] v.10.0.240 into protein families using cut-off values of 80% of protein sequence
449 similarity, 80% of query sequence coverage, e-value equal or less than 0.0001 (parameters -
450 evalue 0.0001 -id 0.8 -query_cov 0.8, with maxaccepts 1 and maxrejects 8). For the core genome
451 various inclusion percentages were compared, since we included draft genomes existing in

452 multiple contigs. The optimum was defined that allowed 3% omissions, giving a species core
453 genome defined as those genes present in 97% of the genome collection. Therefore, protein
454 families with presence in at least 97% of the total set strains were considered part of the core
455 genome of *E. coli* species.

456 The pan- and core genome for each of the 14 phylogroups were then separately clustered using
457 the same cut-off parameters as the entire set at species level.

458

459 ***MLST analysis.*** The sequence type for all 10,667 assembled genomes was assessed using the
460 program "mlst" version 2.18.0 from Seemann T, **Github:** https://github.com/tseemann/mlst,
461 using both the Achtman and Pasteur MLST schemas for *E. coli* from PubMLST website
462 (https://pubmlst.org/) developed[34] by Keith Jolley. Results were collected and are accessible in
463 our microreact database: https://microreact.org/project/10667ecoli/b4431cf8

464 ***Core genome matrix creation and visualization.*** Core genome clusters for the 14 phylogroups
465 obtained using UCLUST v.10.0.240 in the previous analysis were used again with UCLUST
466 v.10.0.240 using the same parameters to find the intersection of core genes between the core
467 clusters of the 14 phylogroups. A binary matrix with cluster ID as column labels, genome IDs as
468 row names, and the number of genes belonging to that cluster as the cell value was constructed
469 using the main output from UCLUST. This matrix was then supplied to an "in house" python
470 script that sorts the pangenome matrix such that the gene clusters found in all phylogroups are
471 placed first (species' core genome). Then groups are sorted by abundance per phylogroup to
472 isolate phylogroup core genes. All leftover gene groups are sorted by phylogroup and abundance
473 and added to the end of the sorted gene cluster list. The Mash tree obtained earlier for the 10,667
474 dataset was then loaded and used to sort the order of the organisms within the sorted matrix.
475 Finally, Matplotlib was used to visualize the sorted matrix.

476 ***Phylogenetic analysis of core gene families.*** The set of core gene clusters of the 14 medoids was
477 extracted from the core genome clusters of the entire species and from them single copy ortholog
478 groups were identified to construct a phylogenomic tree. In total a set of 2,613 single gene

479 (clusters without paralogs paralogs) ortholog groups were aligned using MAFFT[35] v.7.110. The
480 model of evolution for each of the 2,613 protein clusters was calculated using IQ-TREE[36]
481 v.1.6.10 with parameters -m TESTONLY -nt AUTO. Once the best model of evolution was
482 obtained for each of the core protein families, those clusters that shared model of evolution were
483 sent together to IQ-TREE for a better estimation of the substitution model parameters using -m
484 MF+MERGE, -nt AUTO and selecting the final model of evolution with mset parameter. In the
485 last step, all partitions obtained with their corresponding model of evolution were sent again to
486 IQ-TREE for final estimation of the phylogenetic tree for the 14 medoids using ultrafast
487 bootstraping approach (-bb 1000). The resulted core genome tree was re-rooted using the B2-1,
488 B2-2 and G phylogroups branch, according to the results obtained from the Mash analysis and
489 the literature[17] (Gonzalez-Alba *et*. *Al*, 2019).

490 The pangenome matrix needed as input for Count[37] v10.04 for the 14 medoids was constructed
491 using UCLUST (with same parameters for pangenome calculation as in previous analyses). A
492 pivot table was built using the main output from UCLUST and pandas library in a python3 script
493 using the function 'pivot_table' with agglomeration function=sum. Count v10.04 program was
494 used for gene family expansion/contraction analysis, using an optimized gain-loss-duplicated
495 model[38] using Poisson family size distribution, 4 gamma categories for each calculation across
496 families (Edge length, Loss rate, Gain rate and Duplication rate) and different lineage specific
497 variation for gain-loss ratio and duplication-loss ratio between lineages. Measurements were
498 done using 1,000 optimization rounds (reaching convergence before the last iteration) and 0.01
499 convergence threshold on the likelihood.

500 ***Principal Coordinate Analysis.*** The PCoA plot in Fig. 3b was created using R, the entire
501 pangenome matrix for the 10,667 assembled genomes, and the libraries 'ade4' version 1.7-13
502 and 'labdsv' version 2.0-1. A Jaccard distance matrix of the pangenome matrix was created using
503 the 'dist.binary' function from 'ade4'. To create the PCoA data, the Jaccard distance matrix was
504 used in the 'pco' function of 'labdsv' with k = 10,666 (allowing each genome to be a unique
505 dimension). The resultant PCoA data was then graphically rendered using R 'plot' and colors
506 were added by genome classification as shown in Fig. 1.

507 ***Reporting Summary.*** Further information on research design is available in the Nature Research
508 Reporting Summary linked to this article.

509 **Data availability**

510 The data supporting the findings of the study are available in this article, its Supplementary
511 Information files, or from the corresponding author upon request.

512

513 **Code availability**
514 Code is available on GitHub: https://github.com/kalebabram/100k_E_coli_Project

515 **REFERENCES**

516

517 1. Jang, J. *et al.* Environmental *Escherichia coli*: ecology and public health implications-a
518 review. *J. Appl. Microbiol.* **123**, 570–581 (2017).
519 2. Fischer Walker, C. L., Sack, D. & Black, R. E. Etiology of Diarrhea in Older Children,
520 Adolescents and Adults: A Systematic Review. *PLoS Negl. Trop. Dis.* **4**, e768 (2010).
521 3. Dunne, K. A. *et al.* Sequencing a piece of history: complete genome sequence of the original
522 *Escherichia coli* strain. *Microb. Genom.* **3**, mgen000106 (2017).
523 4. Pettengill, E. A., Pettengill, J. B. & Binet, R. Phylogenetic Analyses of *Shigella* and
524 Enteroinvasive *Escherichia coli* for the Identification of Molecular Epidemiological Markers:
525 Whole-Genome Comparative Analysis Does Not Support Distinct Genera Designation. *Front.*
526 *Microbiol.* **6**,1573 (2016).
527 5. Chattaway, M. A., Schaefer, U., Tewolde, R., Dallman, T. J. & Jenkins, C. Identification of
528 *Escherichia coli* and *Shigella* Species from Whole-Genome Sequences. *J. Clin. Microbiol.* **55**,
529 616–623 (2017).

530 6. Clermont, O., Bonacorsi, S. & Bingen, E. Rapid and Simple Determination of the *Escherichia*
531 *coli* Phylogenetic Group. *Appl. Environ. Microbiol.* **66**, 4555–4558 (2000).
532 7. Gordon, D. M., Clermont, O., Tolley, H. & Denamur, E. Assigning *Escherichia coli* strains to
533 phylogenetic groups: multi-locus sequence typing versus the PCR triplex method: MLST
534 versus Clermont method. *Environ. Microbiol.* **10**, 2484–2496 (2008).
535 8. Tenaillon, O., Skurnik, D., Picard, B. & Denamur, E. The population genetics of commensal
536 *Escherichia coli*. *Nat. Rev. Microbiol.* **8**, 207–217 (2010).
537 9. Clermont, O., Christenson, J. K., Denamur, E. & Gordon, D. M. The Clermont *Escherichia coli*
538 phylo-typing method revisited: improvement of specificity and detection of new phylo-
539 groups: A new *E. coli* phylo-typing method. *Environ. Microbiol. Rep.* **5**, 58–65 (2013).
540 10. Meier-Kolthoff, J. P. *et al.* Complete genome sequence of DSM 30083T, the type strain
541 (U5/41T) of *Escherichia coli*, and a proposal for delineating subspecies in microbial
542 taxonomy. *Stand. Genomic Sci.* **9**, 2 (2014).
543 11. Clermont, O. *et al.* Characterization and rapid identification of phylogroup G in *Escherichia*
544 *coli*, a lineage with high virulence and antibiotic resistance potential. *Environ. Microbiol.* **21**,
545 3107–3117 (2019).
546 12. Walk, S. T. *et al.* Cryptic Lineages of the Genus Escherichia. *Appl. Environ. Microbiol.* **75**,
547 6534–6544 (2009).
548 13. Carlos, C. *et al. Escherichia coli* phylogenetic group determination and its application in the
549 identification of the major animal source of fecal contamination. *BMC Microbiol.* **10**, 161
550 (2010).

551 14. Vangchhia, B. *et al.* Phylogenetic diversity, antimicrobial susceptibility and virulence
552 characteristics of phylogroup F *Escherichia coli* in Australia. *Microbiology* **162**, 1904–1912
553 (2016).
554 15. Struyf, A., Hubert, M. & Rousseeuw, P. Clustering in an Object-Oriented Environment. *J.*
555 *Stat. Softw.* **1**, 1-30 (1997).
556 16. Argimón, S. *et al.* Microreact: visualizing and sharing data for genomic epidemiology and
557 phylogeography. *Microb. Genom.* **2**, e000093 (2016).
558 17. Gonzalez-Alba, J. M., Baquero, F., Cantón, R. & Galán, J. C. Stratified reconstruction of
559 ancestral *Escherichia coli* diversification. *BMC Genomics* **20**, 936 (2019).
560 18. Weinert, L. A. & Welch, J. J. Why Might Bacterial Pathogens Have Small Genomes? *Trends*
561 *Ecol. Evol.* **32**, 936–947 (2017).
562 19. Bhunia, A. K. *Escherichia coli*. in *Foodborne Microbial Pathogens: Mechanisms and*
563 *Pathogenesis* (ed. Bhunia, A. K.) 249–269 (Springer New York, 2018). doi:10.1007/978-1-
564 4939-7349-1_14.
565 20. Balbi, K. J., Rocha, E. P. C. & Feil, E. J. The Temporal Dynamics of Slightly Deleterious
566 Mutations in *Escherichia coli* and *Shigella* spp. *Mol. Biol. Evol.* **26**, 345–355 (2009).
567 21. Sharma, V. K., Akavaram, S., Schaut, R. G. & Bayles, D. O. Comparative genomics reveals
568 structural and functional features specific to the genome of a foodborne *Escherichia coli*
569 O157:H7. *BMC Genomics* **20**, 196 (2019).
570 22. Udaondo, Z., Molina, L., Segura, A., Duque, E. & Ramos, J. L. Analysis of the core genome
571 and pangenome of *Pseudomonas putida*. *Environ. Microbiol.* **18**, 3268–3283 (2016).

572 23. Abreo, E. & Altier, N. Pangenome of *Serratia marcescens* strains from nosocomial and
573 environmental origins reveals different populations and the links between them. *Sci. Rep.* **9**,
574 1–8 (2019).
575 24. Salipante, S. J. *et al.* Large-scale genomic sequencing of extraintestinal pathogenic
576 *Escherichia coli* strains. *Genome Res.* **25**, 119–128 (2015).
577 25. Nicolas-Chanoine, M.-H., Bertrand, X. & Madec, J.-Y. *Escherichia coli* ST131, an Intriguing
578 Clonal Group. *Clin. Microbiol. Rev.* **27**, 543–574 (2014).
579 26. Petty, N. K. *et al.* Global dissemination of a multidrug resistant *Escherichia coli* clone. *Proc.*
580 *Natl. Acad. Sci. USA* **111**, 5694–5699 (2014).
581 27. Lecointre, G., Rachdi, L., Darlu, P. & Denamur, E. Escherichia coli molecular phylogeny using
582 the incongruence length difference test. *Mol. Biol. Evol.* **15**, 1685–1695 (1998).
583 28. Ondov, B. D. *et al.* Mash: fast genome and metagenome distance estimation using
584 MinHash. *Genome Biol.* **17**, 132 (2016).
585 29. Land, M. L. *et al.* Quality scores for 32,000 genomes. *Stand. Genomic Sci.* **9**, 20 (2014).
586 30. Wattam, A. R. *et al.* Improvements to PATRIC, the all-bacterial Bioinformatics Database and
587 Analysis Resource Center. *Nucleic Acids Res.* **45**, D535–D542 (2017).
588 31. Pearson's Correlation Coefficient. in *Encyclopedia of Public Health* (ed. Kirch, W.) 1090–
589 1091 (Springer Netherlands, 2008). doi:10.1007/978-1-4020-5614-7_2569.
590 32. Seemann, T. Prokka: rapid prokaryotic genome annotation. *Bioinformatics* **30**, 2068–2069
591 (2014).
592 33. Edgar, R. C. Search and clustering orders of magnitude faster than BLAST. *Bioinformatics* **26**,

593 2460–2461 (2010).

594 34. Jolley, K. A. & Maiden, M. C. BIGSdb: Scalable analysis of bacterial genome variation at the

595 population level. *BMC Bioinformatics* **11**, 595 (2010).

596 35. Katoh, K. & Standley, D. M. MAFFT Multiple Sequence Alignment Software Version 7:

597 Improvements in Performance and Usability. *Mol. Biol. Evol.* **30**, 772–780 (2013).

598 36. Nguyen, L.-T., Schmidt, H. A., von Haeseler, A. & Minh, B. Q. IQ-TREE: A Fast and Effective

599 Stochastic Algorithm for Estimating Maximum-Likelihood Phylogenies. *Mol. Biol. Evol.* **32**,

600 268–274 (2015).

601 37. Csűrös, M. Count: evolutionary analysis of phylogenetic profiles with parsimony and

602 likelihood. *Bioinformatics* **26**, 1910–1912 (2010).

603 38. Csűrös, M. & Miklós, I. Streamlining and Large Ancestral Genomes in Archaea Inferred with

604 a Phylogenetic Birth-and-Death Model. *Mol. Biol. Evol.* **26**, 2087–2095 (2009).

605 **ACKNOWLEDGMENTS**

607 This work was supported by NIH/NIGMS grant 1P20GM121293 and from the Helen Adams &
608 Arkansas Research Alliance Endowment in the Department of Biomedical Informatics, College
609 of Medicine. We thank Dr. Scott Emrich for discussions about Mash in the early stages of this
610 manuscript. We also appreciate the contribution of Dr. Juan Carlos Galan and his group for
611 allowing us to adapt Fig. 3 of their manuscript recently published as Gonzalez-Alba *et al*., 2019
612 into Fig. 2a of our manuscript.

613

614

615

616

Author contributions

K.Z.A and Z.U. conceived and designed all the experiments with help from D.W.U.

K.Z.A and Z.U. conducted all the experiments and drafted the manuscript with contributions from all authors.

C.B. assisted with Cytoscape analysis.

V.W. assisted with the download of SRA reads.

T.M.W. provided advice and discussion and helped with the revision of the manuscript and improvement of figures.

M.S.R. II provided advice, discussion, and assisted with the phylogenetic analysis as well as revising the manuscript and improving figures.

D.W.U. conceived the work, provided funding and provided advice and discussions.

Competing interesting

Author declare no competing interests.

Additional information

Extended data is available for this paper at https://github.com/kalebabram/100k_E_coli_Project

Supplementary information is available for this paper at

Correspondence and request for materials should be addressed to D.W.U.

Reprints and permission information is available at www.nature.com/reprints

646 # Tables

647 **Table 1. Summary of pangenome analysis results.** Values obtained from the different pangenome analysis using
648 the 14 phylogroups separately and the entire set of assembled genomes (10,667 genomes) using UCLUST (Edgar,
649 2010). Same parameters were used to all the analysis.

Phylogroup	Core genome (97% strains)		Accessory genome		Unique		Total (Pan genome)		Core/pan (%)	No. of strains
	clusters	proteins	clusters	proteins	clusters	proteins	clusters	proteins	clusters	
All	2,663	28,566,052	82,821	22,783,754	50,499	51,099	135,983	51,400,905	1.96	10,667
A	3,184	7,142,893	41,769	3,246,591	24,501	24,828	69,454	10,414,312	4.58	2,232
B1	3,141	9,365,646	44,019	4,887,086	24,590	24,844	71,750	14,277,576	4.38	2,960
B2-1	3,708	2,016,812	10,990	619,867	7,048	7,180	21,746	2,643,859	17.05	541
B2-2	3,425	4,709,983	22,762	1,819,538	12,566	12,763	38,753	6,542,284	8.84	1,367
C	3,899	2,132,258	10,413	738,879	5,242	5,290	19,554	2,876,427	19.94	540
D1	3,666	1,006,271	10,012	318,372	7,659	7,770	21,337	1,332,413	17.18	273
D2	3,524	626,693	11,703	221,033	6,765	7,181	21,992	854,907	16.02	177
D3	3,754	668,359	7,252	201,292	4,814	4,936	15,820	874,587	23.73	177
E1	3,151	885,018	14,883	471,354	7,969	8,088	26,003	1,364,460	12.12	279
E2(O157)	4,060	3,080,073	6,128	743,413	4,442	4,535	14,630	3,828,021	27.75	750
F	3,486	698,031	9,465	288,420	5,381	5,480	18,332	991,931	19.02	199
G	3,783	365,756	5,716	98,269	4,016	4,066	13,515	468,091	27.99	96
Shig1	3,128	564,868	4,903	256,426	2,815	2,883	10,846	824,177	28.84	177
Shig2	3,732	3,383,814	6,870	719,247	4,751	4,799	15,353	4,107,860	24.31	899

650

651 **Legends of Tables**

652 **Table 1. Summary of pangenome analysis results.** Values obtained from the different
653 pangenome analysis using the 14 phylogroups separately and the entire set of assembled
654 genomes (10,667 genomes) using UCLUST (Edgar, 2010). Same parameters were used to all the
655 analysis

656 **Legends of Figures**

657 **Fig. 1. Heatmap representation of 10,667 genomes using Mash distances. The color bars at**
658 the top of the heatmap identify the phylogroups as predicted from the analysis. The scale to the
659 left of the dendrogram corresponds to the resultant cluster height of the entire dataset obtained
660 from hclust function in R. The colors in the heatmap are based on the pairwise Mash distance
661 between the genomes. Teal colors represent similarity between genomes with the darkest teal

662 corresponding to identical genomes reporting a Mash distance of 0. Brown colors represent low
663 genetic similarity per Mash distance, with the darkest brown indicating a maximum distance of ~
664 0.039. Genomes of relative median genetic similarity have the lightest color.

665 **Fig. 2. Summary of phylogroup differentiation and heatmap representation of sequence**
666 **reads from the SRA database. a,** Evolutionary scenario in the diversification of *E. coli* adapted
667 from Gonzalez-Alba *et. al*, 2019 based on their methodology "SP-mPH", a combination of
668 "stratified phylogeny" and "molecular polymorphism hallmark". Each branch reflects SNPs
669 accrued by each phylogroup over time. Branch length is not proportional to the observed
670 evolutionary distance. **b,** Summary of the Cytoscape analysis. Phylogroups are colored based on
671 the same colour scheme as Fig. 1. Phylogroups with more than one member are gray coloured.
672 The Mash distance that each division occurs at is indicated by numerical value in the gray bar
673 that runs down the side of this panel. **c,** Clustered heatmap of 91,261sequnce reads. The heatmap
674 colors are based on the pairwise Mash distance between the SRA read sets and the 14 medoid
675 genomes of each phylogroup, which are presented in the same order as in Fig. 1. To be included,
676 SRA reads sets had to have 3 or more medoid comparisons producing a Mash distance equal to
677 or less than 0.04. This removed 4,264 SRA read sets from the dataset. The number of SRA reads
678 mapped to each medoids is given below the heatmap. Supplementary Fig. 2 contains additional
679 cut-offs ranging from one to 14 phylogroups.

680 **Fig. 3. Pangenome representations of *E. coli* and *Shigella*. A**. Each bar length of the circular
681 bar plot represents the total number of proteins of a single genome, grouped by phylogroup. The
682 proteins belonging to the $^{TOT}core_{97}$ genome are shown in green. Additional proteins shared in
683 each $^{PHY}core_{97}$ genome are shown in blue, while purple is reserved for accessory proteins. **B**.
684 Principal Coordinate Analysis plot of 135,983 protein families of 10,667 assembled genomes.
685 Phylogroups are indicated by the same color scheme used in Figs. 1 and 2. **C**. Core genome
686 matrix of 6,719 phylogroup core clusters and 10,667 assembled genomes. Clusters are sorted
687 such that the core for the species is placed first, then the phylogroup core genes are placed sorted
688 by their overall abundance in the species for each phylogroup in the same order as Fig. 1, finally
689 the remaining clusters are placed by overall abundance. Phylogroup unique core genes are
690 indicated by purple blocks which do not appear in other phylogroups.

691 **Fig. 4. Phylogenetic representations of *E. coli* species using the core genome of the 14**
692 **medoids. A.** The tree was built using a set of 2,613 core clusters with no paralogs using IQ-
693 TREE (Nguyen *et al.*, 2015). **B.** Summary representation of Count output. The phylogenetic tree
694 presents the different gain/loss/duplication ratios obtained per each phylogroup as output of
695 Count v.10.04 software (Csűrös, 2010). Dots in branches represent "informative ellipsis" where
696 the length of the undotted section of the branch multiplied by the inverse ratio of undotted
697 section is equal to the true rate of the branch. For example, assuming the displayed branch length
698 is 1 and 1/10th of the branch is solid then the true rate of the branch would be 10.
699 Gain/loss/duplication rates for each branch are shown in the table.

700 **Supplementary Information**

701 **Supplementary Table 1.** 10,667 WGS annotation numbers and strain names used in this study,
702 their metadata and quality scores. This file also includes some of the percent cutoffs and cluster
703 cutoffs tested in this study.

704 **Supplementary Table 2.** Medoid metadata

705 **Supplementary Table 3.** SRA metadata including read name, the predicted phylogroup, the
706 number of hits a read has to phylogroup medoids that is above a cutoff of 0.04.

707 **Supplementary Table 4.** Results of the ANOVA and Tukey's test for the analysis of the means
708 of genome sizes and GC content per phylogroup.

709 **Supplementary Table 5.** Functional annotation using KO terms per each of the clusters found as
710 phylogroup unique core genes

711

712 **Supplementary Figures**

713 **Supplementary Figure 1.** Distribution of *Shigella* genomes over phylogroups.

714 **Supplementary Figure 2.** Heatmaps of all SRA reads that had a Mash score of at least 0.04 to
715 one medoid. Each heatmap has a set of genomes with at least the indicated number of hits to a
716 medoid of at least 0.04.

717 **Supplementary Figure 3.** Violin-plots of the distribution of genome size (A) and genomic GC
718 content (B) by phylogroup. Bar-plots inside the violins represent values for mean and mean plus
719 one standard deviation per phylogroup. Phylogroups that have values significantly different to all

720 other phylogroups (according to F statistics test) are marked with a red asterisk.

721 **Supplementary Figure 4.** Cut-offs for core genome calculation. Core genomes established at a
722 cutoff of 90% to 100% per phylogroup. Last section represents the rate of cluster drop-off
723 between percentages (90% to 99%)

724

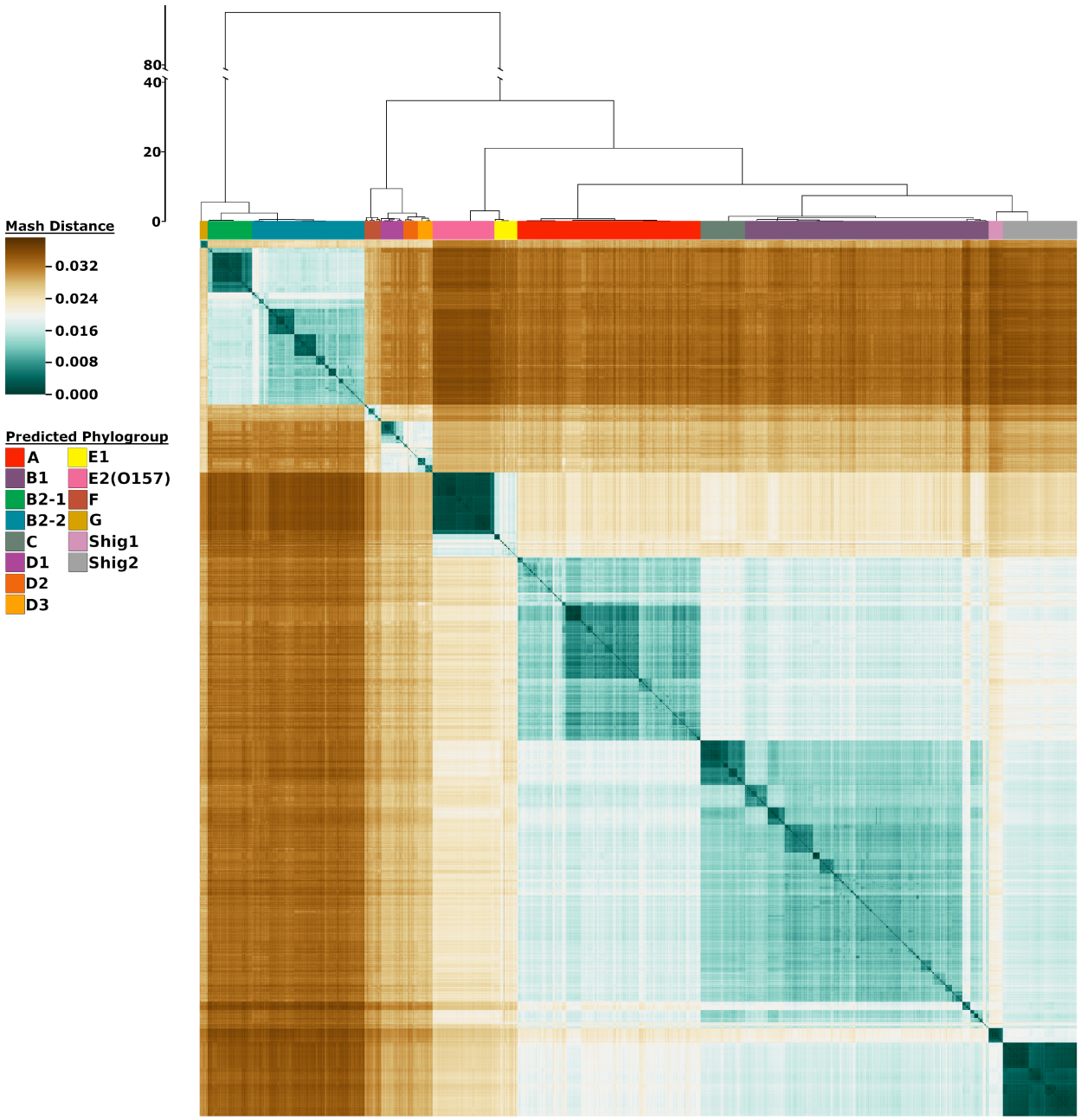

Fig. 1. Heatmap representation of 10,667 genomes using Mash distances. The color bars at the top of the heatmap identify the phylogroups as predicted from the analysis. The scale to the left of the dendrogram corresponds to the resultant cluster height of the entire dataset obtained from hclust function in R. The colors in the heatmap are based on the pairwise Mash distance between the genomes. Teal colors represent similarity between genomes with the darkest teal

corresponding to identical genomes reporting a Mash distance of 0. Brown colors represent low genetic similarity per Mash distance, with the darkest brown indicating a maximum distance of ~ 0.039. Genomes of relative median genetic similarity have the lightest color.

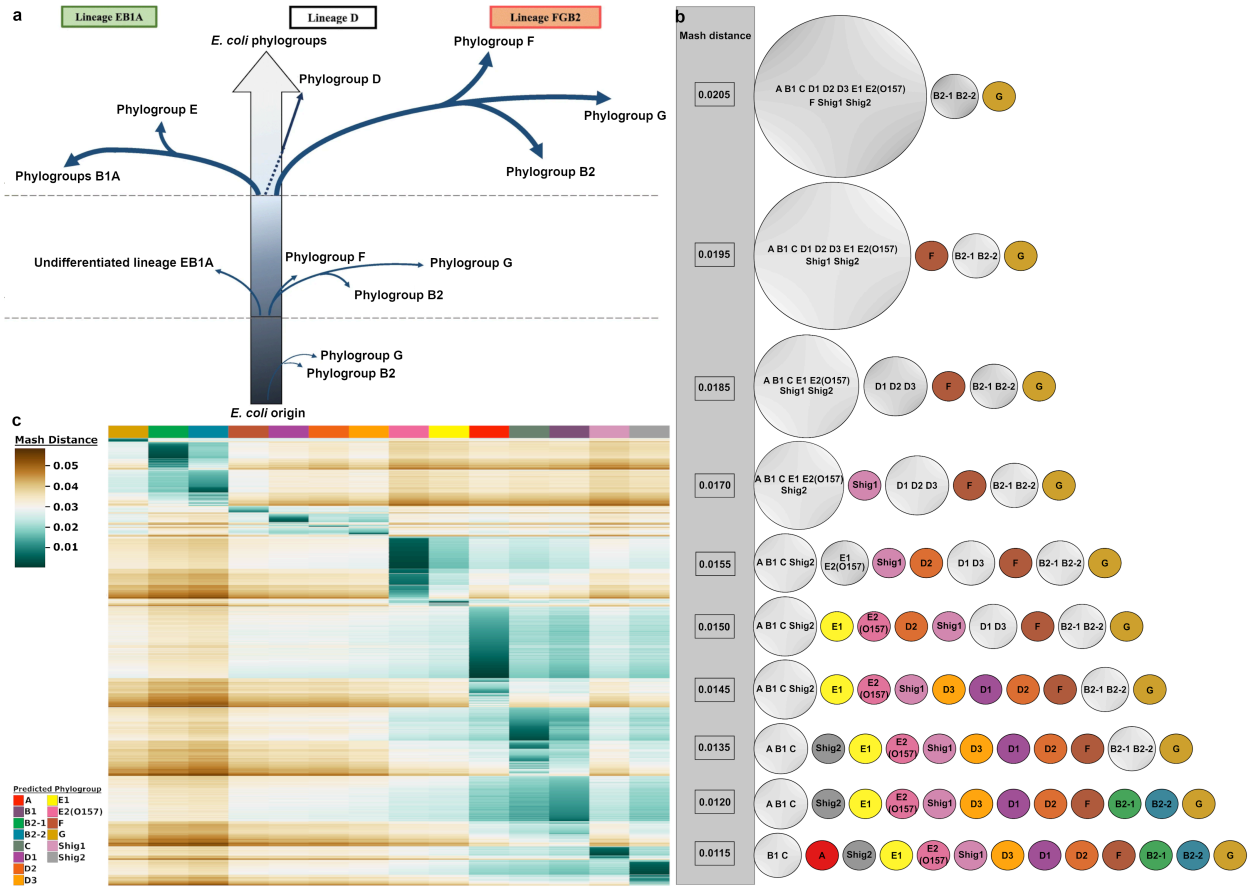

Fig. 2. Summary of phylogroup differentiation and heatmap representation of sequence reads from the SRA database. a, Evolutionary scenario in the diversification of *E. coli* adapted from Gonzalez-Alba *et. al*, 2019 based on their methodology "SP-mPH", a combination of "stratified phylogeny" and "molecular polymorphism hallmark". Each branch reflects SNPs accrued by each phylogroup over time. Branch length is not proportional to the observed evolutionary distance. **b,** Summary of the Cytoscape analysis. Phylogroups are colored based on the same colour scheme as Fig. 1. Phylogroups with more than one member are gray coloured. The Mash distance that each division occurs at is indicated by numerical value in the gray bar that runs down the side of this panel. **c,** Clustered heatmap of 91,261sequnce reads. The heatmap colors are based on the pairwise Mash distance between the SRA read sets and the 14 medoid genomes of each phylogroup, which are presented in the same order as in Fig. 1. To be included, SRA reads sets had to have 3 or more medoid comparisons producing a Mash distance equal to or less than 0.04. This removed 4,264 SRA read sets from the dataset. The number of SRA reads

764 mapped to each medoids is given below the heatmap. Supplementary Fig. 2 contains additional
765 cut-offs ranging from one to 14 phylogroups.

766

767

768

769

770

771

772

773

774

775

776

777

778

779

780

781

782

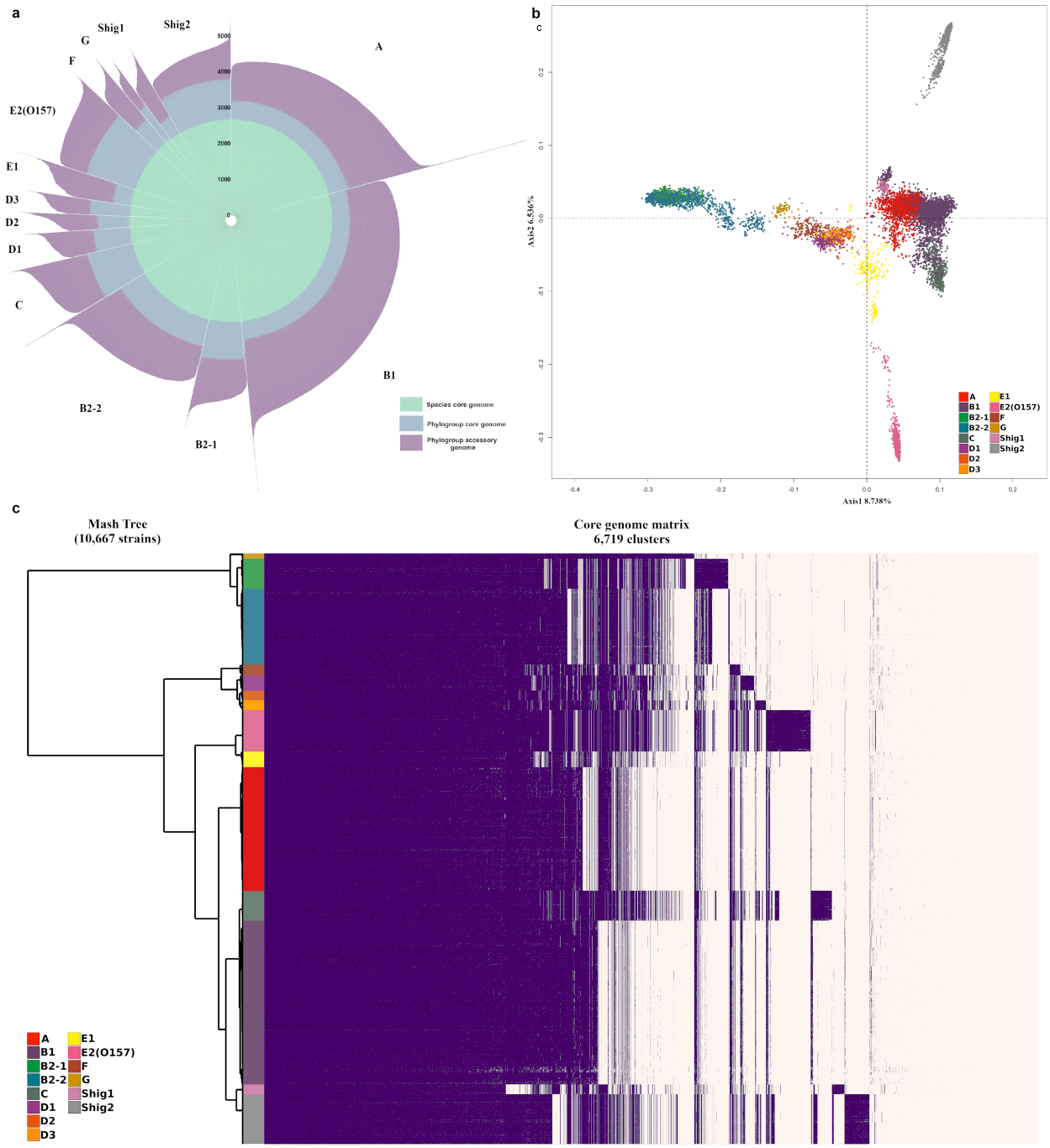

783

784 **Fig. 3. Pangenome representations of *E. coli* and *Shigella*. A**. Each bar length of the circular
785 bar plot represents the total number of proteins of a single genome, grouped by phylogroup. The
786 proteins belonging to the $^{TOT}core_{97}$ genome are shown in green. Additional proteins shared in
787 each $^{PHY}core_{97}$ genome are shown in blue, while purple is reserved for accessory proteins. **B**.

788 Principal Coordinate Analysis plot of 135,983 protein families of 10,667 assembled genomes.
789 Phylogroups are indicated by the same color scheme used in Figs. 1 and 2. **C**. Core genome
790 matrix of 6,719 phylogroup core clusters and 10,667 assembled genomes. Clusters are sorted
791 such that the core for the species is placed first, then the phylogroup core genes are placed sorted
792 by their overall abundance in the species for each phylogroup in the same order as Fig. 1, finally
793 the remaining clusters are placed by overall abundance. Phylogroup unique core genes are
794 indicated by purple blocks which do not appear in other phylogroups.

795

796

797

798

799

800

801

802

803

804

805

806

807

808

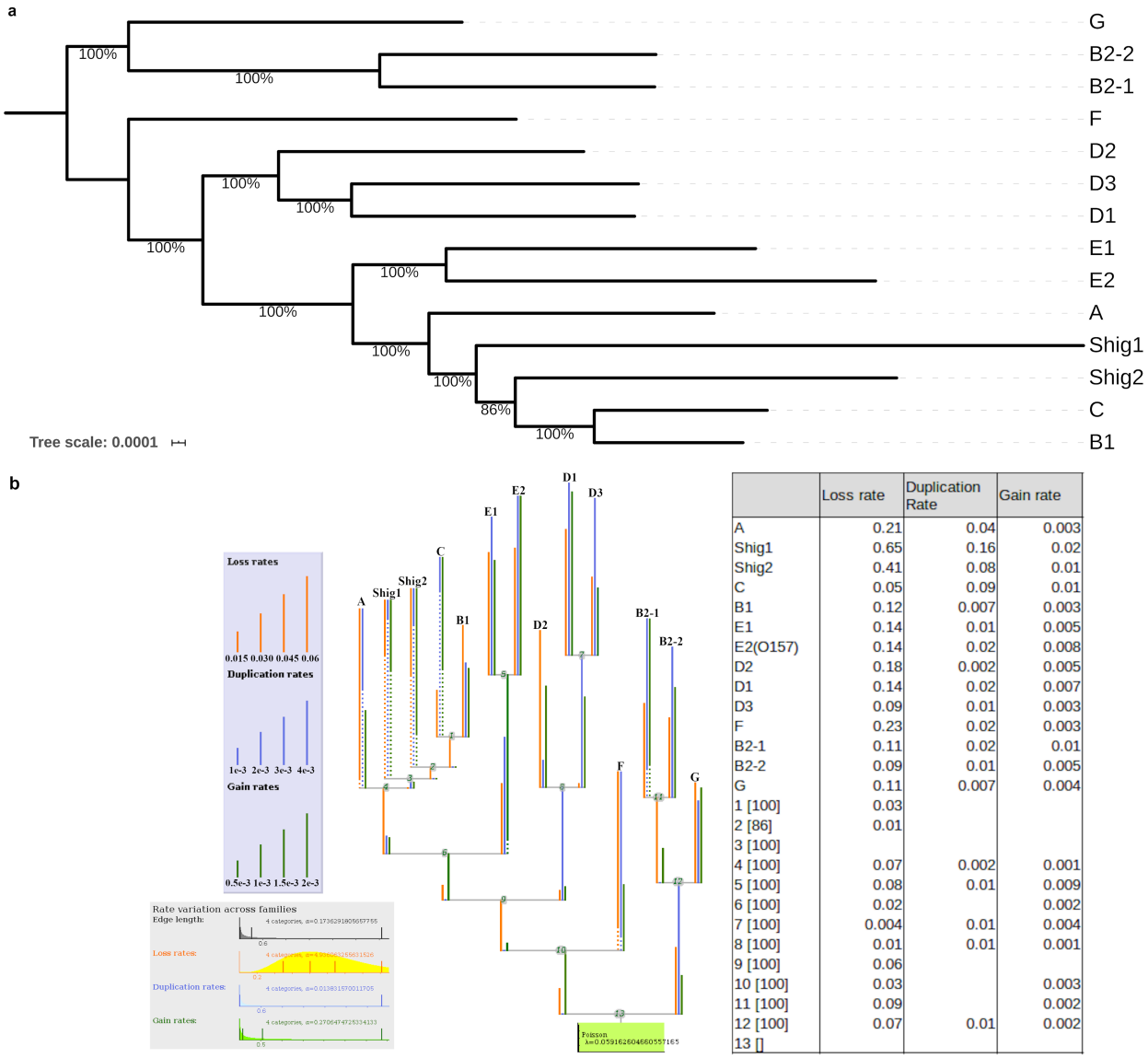

	Loss rate	Duplication Rate	Gain rate
A	0.21	0.04	0.003
Shig1	0.65	0.16	0.02
Shig2	0.41	0.08	0.01
C	0.05	0.09	0.01
B1	0.12	0.007	0.003
E1	0.14	0.01	0.005
E2(O157)	0.14	0.02	0.008
D2	0.18	0.002	0.005
D1	0.14	0.02	0.007
D3	0.09	0.01	0.003
F	0.23	0.02	0.003
B2-1	0.11	0.02	0.01
B2-2	0.09	0.01	0.005
G	0.11	0.007	0.004
1 [100]	0.03		
2 [86]	0.01		
3 [100]			
4 [100]	0.07	0.002	0.001
5 [100]	0.08	0.01	0.009
6 [100]	0.02		0.002
7 [100]	0.004	0.01	0.004
8 [100]	0.01	0.01	0.001
9 [100]	0.06		
10 [100]	0.03		0.003
11 [100]	0.09		0.002
12 [100]	0.07	0.01	0.002
13 []			

Fig. 4. Phylogenetic representations of *E. coli* species using the core genome of the 14 medoids. A. The tree was built using a set of 2,613 core clusters with no paralogs using IQ-TREE (Nguyen *et al.*, 2015). **B.** Summary representation of Count output. The phylogenetic tree presents the different gain/loss/duplication ratios obtained per each phylogroup as output of Count v.10.04 software (Csűrös, 2010). Dots in branches represent "informative ellipsis" where the length of the undotted section of the branch multiplied by the inverse ratio of undotted section is equal to the true rate of the branch. For example, assuming the displayed branch length is 1 and 1/10th of the branch is solid then the true rate of the branch would be 10.

818 Gain/loss/duplication rates for each branch are shown in the table.

819